Diagnosis of Autism Spectrum Disorder Based on Eigenvalues of Brain Networks

SAKIB MOSTAFA[1], LINGKAI TANG[2], AND FANG-XIANG WU[1,2,3]
[1]Division of Biomedical Engineering, University of Saskatchewan, Saskatoon, SK S7N 5A9, Canada
[2]Department of Mechanical Engineering, University of Saskatchewan, Saskatoon, SK S7N 5A9, Canada
[3]Department of Computer Science, University of Saskatchewan, Saskatoon, SK S7N 5A9, Canada

Corresponding author: Fang-Xiang Wu (faw341@mail.usask.ca)

ABSTRACT Autism spectrum disorder (ASD) is a neuro dysfunction which causes the repetitive behavior and social instability of patients. Diagnosing ASD has been of great interest. However, due to the lack of discriminate differences between neuroimages of healthy persons and ASD patients, there has been no powerful diagnosis approach. In this study, we have designed brain network-based features for the diagnosis of ASD. Specifically, we have used the 264 regions based parcellation scheme to construct a brain network from a brain functional magnetic resonance imaging (fMRI). Then we have defined 264 raw brain features by the 264 eigenvalues of the Laplacian matrix of the brain network and another three features by network centralities. By applying a feature selection algorithm, we have obtained 64 discriminate features. Furthermore, we have trained several machine learning models for diagnosing ASD with our obtained features on ABIDE (Autism Brain Imaging Data Exchange) dataset. With our derived features, the linear discriminant analysis has achieved the classification accuracy of 77.7%, which is better than the state-of-the-art results.

INDEX TERMS Brain network, feature, eigenvalue, network centrality, functional magnetic resonance imaging, machine learning.

LIST OF ABBREVIATIONS

ABIDE	Autism Brain Imaging Data Exchange
ACC	Accuracy
AFNI	Analysis Of Functional Neuroimages
ASD	Autism Spectrum Disorder
AUC	Area Under ROC Curve
CSF	Cerebrospinal Fluid
fMRI	Functional MRI
FSL	FMRIB's Software Library
FWHM	Full-Width Half Maximum
KNN	K Nearest Neighbor
LDA	Linear Discriminant Analysis
LR	Logistic Regression
MRI	Magnetic Resonance Imaging
NN	Neural Network
PCC	Pearson Correlation Coefficient
ROC	Receiver Operating Characteristic
ROI	Region of Interest
rs-fMRI	Resting State Functional MRI
STDV	Standard Deviation
SVM	Support Vector Machine
TC	Typical Controls
WM	White Matter

I. INTRODUCTION

Autism spectrum disorder (ASD) is a neuro dysfunction found in children. Children who are affected by ASD have difficulties in their social life, verbal and non-verbal communications and sometimes have repetitive patterns of behaviors. According to the 2018 National Autism Spectrum Disorder Surveillance System report [1], 1 in 66 children in Canada suffers from ASD. Apart from the behavioral abnormality, there are no other perceptible symptoms for effectively diagnosing ASD. To diagnose ASD, patients traditionally need to go through behavioral observation or interview such as Autism Diagnostic Observation Schedule [2], Autism Diagnostic Interview [3]. However, recently, the use of machine learning classifiers to classify between ASD patients and typical controls (TC) has been attractive. The performance of machine learning algorithms depends on

the features or biomarkers that are used for the classification. Different features such as structural properties of brains [4], phenotype information [5], [6], behavioral attributes [7] have been used to classify between ASD and TC. However, in most of the cases, these features are not sufficient enough to diagnose ASD accurately. Machine learning classifiers can perform well when information from neuroimage data are used as features [8].

Magnetic Resonance Imaging (MRI) provides information about the structure, functional activity, and composition of brains [9]. The resting state functional MRI (rs-fMRI) images are now very popular for studying brain diseases because they can be obtained in a non-invasive way and also provide information about interactions among brain regions [10], [11]. This helps understand the neural activities of a person's brain, which has neuro-developmental disorders [12]. Rather than studying the rs-fMRI images a more powerful and flexible way is the graph-theoretic or network approach [13], [14]. A network consists of nodes and the edges linking the pair of nodes.

In network-based approaches for analyzing fMRI, the whole brain is divided into a number of regions of interest (ROIs), which are the nodes in a brain network. Then time-series measurements of functional activities of ROIs are used to compute the cross-correlation as the connection strength among ROIs, which are the edges of a brain network. A brain network can be represented by its connectivity matrix, where each element of the matrix represents the cross-correlation of the time-series measurements between the corresponding ROIs. The connectivity matrix has been used in various ways to classify ASD and TC. In the study [15], for the classification of ASD and TC, the correlation values of all pairwise ROIs are used as features for a probabilistic neural network. The intrinsic connectivity of the brain of children is studied in [16] to detect the marker ROIs of ASD. The group [17] have defined each gray matter voxel as an ROI and have used their classification algorithm on the connectivity matrix for the detection of brain diseases. The connectivity matrix has also been used to study the functional and structural properties of brains in [18].

There have been many studies regarding the diagnosis of ASD using machine learning approaches. The group in [19] have achieved a classification accuracy of 75.3% by decomposing the ROIs of each subject with the double-density dual-tree discrete wavelet transform into the time-frequency sub-bands and then using generalized autoregressive conditional heteroscedasticity to select features from the sub-bands. However, out of the 1112 subjects over 17 different sites in the Autism Brain Imaging Data Exchange 1 (ABIDE 1) dataset, the study has only included 468 subjects from six different sites of ABIDE 1. In [20], a classification accuracy of 72.6% and 71.4% is achieved with a sparse multiview task-centralized ensemble classification method for the NYU and UM1 dataset, respectively, from the ABIDE 1. There are only 183 and 96 subjects in NYU and UM1,

respectively. Also, the study has only reported results for conducting the experiments separately on individual sites. The classification accuracy of as high as 96.5% is reported in [21], using only the USM dataset containing 50 subjects. In [22], the elements of the connectivity matrix is used directly in the machine learning classifier for the diagnosis of ASD. To evaluate their method, they have used two datasets: ABIDE 1 with 88 subjects and a Japanese dataset with 181 subjects. The results have shown that their method achieves a classification accuracy of 85.0% and 71.0%, respectively.

Apart from the single-site classification, there are studies where the researchers use the data from all the sites in ABIDE 1. Combining the phenotypic information of the subjects with the time-series information from the rs-fMRI images in [6], a classification accuracy of 70.1% is achieved on the entire ABIDE 1 dataset. A deep learning-based approach in [23] has reported a classification accuracy of 70.0%. They have used two stacked denoising autoencoder to pre-train a deep neural network. The input of the network is the Pearson correlation coefficient (PCC) of all pairwise ROIs. They have also conducted experiments for single-site data and reported an average classification accuracy of 52.0%. The classification accuracy of 71.1% is reported in [8] where connectivity matrices under the log-Euclidean and affine-invariant Riemannian metrics are used in machine learning algorithms. A more recent study [24] has used autoencoder to pre-train a single layer perceptron for the diagnosis of ASD. They have achieved the classification accuracy of 70.1% for the entire ABIDE 1 dataset and an average accuracy of 63.0% for individual sites.

The study in [25] has shown that the classification accuracy of the machine learning-based ASD diagnosis process tend to be higher when the sample size (number of subjects) is smaller. The classification accuracy decrease with the increase of the sample size, which is evident from the above discussion. The studies have low classification accuracy because the features used in the studies aren't discriminate enough to diagnose ASD. Therefore, it is necessary to define discriminate features which can diagnose ASD with a high classification accuracy using the entire ABIDE 1 dataset.

In this study, we propose the eigenvalues of the Laplacian matrix of a brain network as new features to diagnose ASD (classify ASD and TC subjects) more accurately. At first, we have adopted the 264 regions based parcellation scheme [26] to divide a brain cortex into 264 ROIs and extracted time-series measurements of these ROIs to create the connectivity matrix. To create features for machine learning algorithms, we have extracted 264 eigenvalues from the Laplacian matrix of a connectivity matrix and combined them with three network centralities: the assortativity, clustering coefficient, and the average degree. To avoid the overfitting problem and select discriminate features for machine learning algorithms, a sequential feature selection algorithm is applied to these 267 features. Then to investigate the classification capability of the newly defined features we have applied them with different machine learning algorithms on ABIDE 1

TABLE 1. Scanning parameters of different sites of ABIDE 1.

Sites	MRI Scanner	TR (ms)		TE (ms)		Flip Angle (Degree)		Voxel Size (mm)	
		A	F	A	F	A	F	A	F
CALTECH	SIEMENS	1590	2000	2.73	30	10	75	1.0×1.0×1.0	3.50×3.50×3.50
CMU	SIEMENS	1870	2000	2.48	30	8	73	1.0×1.0×1.0	3.00×3.00×3.00
KKI	PHILLIPS	8	2500	3.70	30	8	75	1.0×1.0×1.0	3.05×3.15×3.00
MAX_MUN	SIEMENS	1800	3000	3.06	30	9	80	1.0×1.0×1.0	3.00×3.00×4.00
NYU	SIEMENS	2530	2000	3.25	15	7	90	1.3×1.0×1.3	3.00×3.00×4.00
OLIN	SIEMENS	2500	1500	2.74	27	8	60	1.0×1.0×1.0	3.40×3.40×4.00
OHSU	SIEMENS	2300	2500	3.58	30	10	90	1.0×1.0×1.0	3.80×3.80×3.80
SDSU	GE	11.08	2000	4.3	30	45	90	1.0×1.0×1.0	3.40×3.40×3.40
SBL	PHILLIPS	9	2200	3.50	30	8	80	1.0×1.0×1.0	2.75×2.75×2.72
STANFORD	GE	8.4	2000	1.80	30	15	80	0.8×1.5×0.8	3.12×3.12×4.50
TRINITY	PHILLIPS	8.5	2000	3.80	28	8	90	1.0×1.0×1.0	3.00×3.00×3.50
UCLA	SIEMENS	2300	3000	2.84	28	9	90	1.0×1.0×1.2	3.00×3.00×4.00
LEUVEN	PHILLIPS	9.6	1656	4.6	33	8	90	0.9×0.9×1.2	3.59×3.59×4.00
UM	GE	250	2000	1.8	30	15	90	1.0×1.0×1.0	3.43×3.43×3.00
PITT	SIEMENS	2100	1500	3.93	25	7	70	1.1×1.1×1.1	3.10×3.10×4.00
USM	SIEMENS	2300	2000	2.91	28	9	90	1.0×1.0×1.2	3.40×3.40×3.00
YALE	SIEMENS	1230	2000	1.73	25	9	60	1.0×1.0×1.0	3.40×3.40×4.00

A: Anatomical, **F**: Functional, **CALTECH**: California Institute of Technology, **CMU**: Carnegie Mellon University, **KKI**: Kennedy Krieger Institute, **MAX_MUN**: Ludwig Maximilians University Munich, **NYU**: NYU Langone Medical Center, **OLIN**: Olin, Institute of Living at Hartford Hospital, **OHSU**: Oregon Health and Science University, **SDSU**: San Diego State University, **SBL**: Social Brain Lab BCN NIC UMC Groningen and Netherlands Institute for Neurosciences, **STANFORD**: Stanford University, **TRINITY**: Trinity Centre for Health Sciences, **UCLA**: University of California, Los Angeles, **LEUVEN**: University of Leuven, **UM**: University of Michigan, **PITT**: University of Pittsburgh School of Medicine, **USM**: University of Utah School of Medicine, **YALE**: Yale Child Study Center.
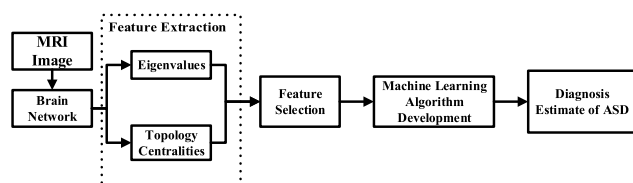

FIGURE 1. Illustration of the main steps of diagnosing ASD. MRI images are processed to create brain networks for individual subjects. New features are extracted from brain networks. After the feature selection, discriminate features are determined for machine learning algorithms.

dataset to diagnose ASD. The Linear Discriminant Analysis (LDA) with these features has reached a classification accuracy of 77.7%, which is better than the state-of-the-art methods [8], [6], [23], [27], [28], [29], [30]. The framework of our method is illustrated in Fig. 1.

II. MATERIALS AND METHODS

A. ABIDE DATASET

Researchers on the diagnosis of ASD have not used a consistent dataset to make their work compatible and comparable with others. Also, the samples used in most studies are not sufficient or diverse enough to validate their proposed methods. To make our study comparable with the available studies we have used the ABIDE 1 dataset [31]. The ABIDE 1 consists of rs-fMRI images, structural MRI images (T1-weighted) and phenotypic information of the 1112 subjects, among which 539 are ASD while 573 are TC

subjects. The data are collected from 17 different sites and stored together. The ABIDE 1 dataset is a very complicated dataset to work with because of the heterogeneity of the subjects (samples). The variances between inter-site data are pretty significant as different sites of ABIDE 1 acquired their data independently and used different scanners or scanning parameters. In Table 1, the details about the scanning parameters are given. To make our study consistent with existing studies [8], [27], [29], we have used the same 871 samples from the ABIDE 1 dataset. Out of 871 subjects, 403 are ASD subjects while 468 are TC subjects. The phenotypic information of 871 samples is given in Table 2. As we can see from both Table 1 and Table 2, the ABIDE 1 dataset covers a wide range of scanning parameters and subject ages. As a result, there is very less similarity between intra-site data, which makes it so hard to work with.

B. MRI DATA PREPROCESSING

Before any downstream analysis, some preprocessing should be applied to rs-fMRI images. We have used AFNI (Analysis of Functional NeuroImages) [32] and FSL (FMRIB's Software Library) [33] for the image preprocessing. Both of them have a wide range of toolboxes for the neuroimaging analysis. Our preprocessing pipeline uses both structural (T1-weighted) and functional (rs-fMRI) images. At first, we have removed the spikes in time series measurements caused by the sudden movements of subjects using an AFNI function called **3dDespike**. Then **3dAutomask** and **3dSkull-Strip** of AFNI are used to remove the skull to acquire only

Sites	Age (Years)	Count		Total
		ASD	TC	
CALTECH	17.0 - 56.2	5	10	15
CMU	19.0 − 40.0	6	5	11
KKI	8.0 - 12.8	12	21	33
MAX_MUN	7.0 − 58.0	19	27	46
NYU	6.5 - 39.1	74	98	172
OLIN	10.0 − 24.0	14	14	28
OHSU	8.0 - 15.2	12	13	25
SDSU	8.7 - 17.2	8	19	27
SBL	20.0 − 64.0	12	14	26
STANFORD	7.5 - 12.9	12	13	25
TRINITY	12.0 - 25.9	19	25	44
UCLA 1	8.4 - 17.9	37	27	64
UCLA 2	9.8 - 16.5	11	10	21
LEUVEN 1	18.0 − 32.0	14	14	28
LEUVEN 2	12.1 - 16.9	12	16	28
UM 1	8.2 - 19.2	34	52	86
UM 2	12.8 - 28.8	13	21	34
PITT	9.3 - 35.2	24	26	50
USM	8.8 - 50.2	43	24	67
YALE	7.0 - 17.8	22	19	41
Total		403	468	871

brain images from functional and structural MRI images, respectively. After that, we have used the **MCFLIRT** function of FSL, to correct motions in the functional volumes on specific time series and calculated the mean functional volume. For MCFLIRT, the normalized correlation ratio is used as the cost function, and the sinc interpolation is used for resampling to increase the classification accuracy by increasing the resolution of images [34]. **FLIRT** of FSL is used to register rs-fMRI images to the standard space MNI 152, which is a high-dimensional nonlinear average registration of 152 T1-weighted MRI images. At first, an rs-fMRI image is registered to its corresponding T1-weighted image. Then the T1-weighted image is registered to the MNI 152 standard space [34], [35]. The full width half maximum (FWHM) Gaussian kernel of 5mm is then applied to make the images smoother. To align the volumes of each time series, images are rotated, translated, scaled, and skewed in X, Y, and Z directions of the MNI 152 standard space. We have then regressed out the six parameters of rigid body movements, i.e., rotation and translation in the X, Y, and Z directions, to minimize the effect of body movements. We have also regressed out the average white matter (WM) and cerebrospinal fluid (CSF). For this process, at first a T1-weighted image is segmented using **FAST** of FSL [36] and then **3dMaskave** of AFNI is used to calculate the average of the time-series measurements. After that, the regression of six rigid body movements, WM and CSF are done by AFNI functions **3dConvolve** and **3dREMLfit**. To decry the effects caused by the heartbeat and respiration a bandpass filter with the passband of 0.01Hz to 0.1Hz is applied to the image.

C. BRAIN NETWORKS

As mentioned, a network consists of nodes and edges while nodes are connected by edges. To construct a network

representing a human brain from MRI images, one of the common problems is defining nodes and edges [37], [38] on which the complexity of a network depends. If nodes and edges are not defined properly, the network might become too complex to analyze [39]. Two of the most popular approaches to define a network are voxel-based approaches [34], [35] and ROI based parcellation schemes [23], [27]. In a voxel-based approach, each voxel of an MRI image is considered as a node and the connection between each voxel is as an edge [42], [43]. However, in this approach, it is ignored that ROIs rather than very small portions (voxels) contribute to the functionality of brain [44], [45]. In an ROI based parcellation scheme, a brain is divided into a number of ROIs. Each ROI is considered to be a node, and connections between ROIs are edges. ROIs can be defined anatomically, which means ROIs are based on some anatomical part of a brain, i.e. amygdala, cortex, sulci, gyri, and so on [34], [43]–[45]. There is also some predefined anatomical atlas popular in studies of neuroimages, where the cortex is partitioned based on the anatomical features. Desikan atlas containing 34 cortical ROIs in each hemisphere [48], Automated Anatomical Labeling atlas [49] containing 116 ROIs, DKT 40 atlas [50], Destrieux atlas [51] are some of the predefined atlases. These atlases work well to build structural networks based on the structural property of brains [50]–[53]. Also, these atlases cover large brain regions in their mentioned ROIs, and large brain regions contain multiple functional regions which can make the network complicated and distort the actual property of brain networks [26], [39]. In this study, we adopt the 264 ROIs based parcellation scheme, as proposed in [26]. These 264 regions are selected because these regions are found active in fMRI images when participants were asked to perform specific tasks. With this parcellation scheme, we have divided a brain into 264 ROIs, and each ROI is defined as a 5mm sphere centered at the MNI coordinate point of 264 regions. Using the FSL **FLIRT** they are then registered to the functional space. These 264 ROIs consists of all the nodes of a brain network.

In a brain network, an edge indicates a particular relationship between a pair of nodes. In the structure network derived from T1-weighted images, an edge between two nodes is weighted by the number of fibers between two ROIs [18]. In a functional brain network derived from rs-fMRI images, an edge between two ROIs is typically weighted by the PCC of the time series measurements [56]. The PCC, r_{xy} between two time series x and y is calculated as follows

$$r_{xy} = \frac{\sum_{b=1}^{s}(x_b - \overline{x})(y_b - \overline{y})}{\sqrt{\sum_{b=1}^{s}(x_b - \overline{x})^2}\sqrt{\sum_{b=1}^{s}(y_b - \overline{y})^2}} \quad (1)$$

where s is the length of time series, x_b and y_b are the b-th component of x and y, respectively, $\overline{x}$ and $\overline{y}$ are the means of x and y, respectively. The PCC ranges from $+1$ to -1. The positive PCC value is interpreted as both the ROIs are

similarly active at the same time for the same neural cause. The more the similarity of the activation, the larger the PCC value is. On the other hand, a negative PCC value means the activation of ROIs are different, i.e., one ROI is more or less active than the other one [57], and it increases with the dissimilarity of the activation of ROIs.

To represent a brain network we have derived a 264×264 connectivity matrix, where each row or column corresponds to a node in the network, and each element is the edge weight between two corresponding nodes.

D. FEATURE EXTRACTION AND FEATURE SELECTION

Rather than analyzing a connectivity matrix directly, a common approach is to threshold the connectivity matrix and remove edges with negative PCC values. The biological significance behind this approach is that positively correlated ROIs tend to cluster together, which gives information about ROIs responsible for neural functions [58], [59]. However, it is shown in [58]–[60], negatively correlated ROIs can be incorporated into the study to get a better understanding of neural activities. In our study, we have taken into account the contribution of both the positive and negative edges, i.e., edges representing positive PCC values and negative PCC values, respectively. Because a negative correlation doesn't mean that there is no connection between ROIs. Instead it indicates ROIs have an anti-correlation [61]–[63]. Further, the thresholding can be applied to the connectivity matrix to remove weak edges, i.e. edges with small absolute PCC values. In practices, thresholding a connectivity matrix to remove weak edges plays a significant role in how a network is going to be defined, which affects the features that are extracted from the network. If no thresholding is applied to the connectivity matrix, then all the regions are connected with each other. The contribution of a weak edge and a strong edge (edges representing large absolute PCC values) is considered the same, which may not be reasonable. Thresholding the weak edges disconnects some ROIs from each other. Increasing the threshold value, more ROIs are disconnected from each other. In this study, for n nodes, we have computed an adjacency matrix, $A = (a_{i,j})_{n \times n}$ by thresholding the elements of the connectivity matrix, $CM = (cm_{i,j})_{n \times n}$ using different threshold values $T > 0$, as follows

$$a_{i,j} = \begin{cases} 1, & if \ cm_{i,j} \geq T \\ -1, & if \ cm_{i,j} \leq -T \\ 0, & if \ i = j \\ 0, & otherwise \end{cases} \quad (2)$$

From the adjacency matrix, we have calculated the degree matrix, $D = (d_{i,j})_{n \times n}$ as follows

$$d_{i,j} = \begin{cases} \sum_{j=1}^{n} a_{i,j}, & if \ i = j \\ 0, & otherwise \end{cases} \quad (3)$$

The Laplacian matrix, $L = (l_{i,j})_{n \times n}$ which is the difference between the degree matrix D and the adjacency matrix A and

it is calculated as follows

$$l_{i,j} = \begin{cases} d_{i,j}, & if \ i = j \\ -a_{i,j}, & if \ i \neq j \end{cases} \quad (4)$$

Features are extracted from these matrices for training the classifiers. Specifically, eigenvalues are calculated with the Laplacian matrix and all the other features are calculated with the adjacency matrix.

1) EIGENVALUES
The eigenvalues λ of a matrix M can be obtained by solving its following characteristic equation

$$P(\lambda) = \det(M - \lambda I) = 0 \quad (5)$$

where I is an identity matrix with the same size of M. The spectrum (set of all eigenvalues of a matrix) is a representation of the key information in a matrix. The spectrum is unique for any given matrix. It is shown in [66] that spectra can be used to measure the similarity. Specifically, if the spectra of the two matrices are strongly correlated, then the matrices are very similar or strongly correlated.

The connectivity matrix is a representation of a brain network of a subject. All brain networks of subjects with ASD should be more similar than those with TC, and vice versa. Therefore, spectra calculated from connectivity matrices of all ASD subjects are more similar than those with TC subjects, and vice versa.

In [18], [67], different centralities are studied for the diagnosis of ASD, but the classification accuracy is poor. It indicates a more discriminant set of features can increase the classification accuracy. In this study, we have defined the spectra of Laplacian matrices as a large part of raw features for machine learning algorithms to establish a better ASD diagnosis process with a higher classification accuracy.

2) TOPOLOGY CENTRALITIES
Besides the spectra of the Laplace matrix, we have also used the topological properties of a network as features. We have calculated several topology centralities of brain network such as global and local efficiency, average path length, graph strength, assortativity, clustering coefficient, and the average degree of a network. However, after the feature selection algorithm (in Section 3) along with the part of spectra, only the assortativity, the clustering coefficient, and the average degree are included in the final feature set. Therefore, in the following, we only describe how to calculate these three centralities.

a: ASSORTATIVITY
The assortativity (denoted by ρ) evaluates the propensity of nodes to associate with each other based on their degree inside a network [68], and it is calculated as the cross-correlation of the degree of every pair of the nodes connected through an edge. To measure the assortativity at first the adjacency matrix A for n nodes is transformed to $\overline{A} = (\overline{a}_{i,j})_{n \times n}$ as

follows

$$\overline{a}_{i,j} = \begin{cases} 1, & if \ a_{i,j} > 0 \\ 0, & otherwise \end{cases} \tag{6}$$

Then the assortativity is calculated as follows

$$\rho = \frac{\frac{1}{k}(\sum_{i,j\in V} d_i.d_j) - \left[\frac{1}{k}(\sum_{i,j\in V} \frac{1}{2}(d_i.d_j))\right]^2}{\frac{1}{k}(\sum_{i,j\in V} \frac{1}{2}(d_i^2 + d_j^2)) - \left[\frac{1}{k}\left(\sum_{i,j\in V} \frac{1}{2}(d_i + d_j)\right)\right]^2} \tag{7}$$

where V is the set of nodes and E is the set of edges, i and j are any two nodes in the upper triangle of $\overline{A}$ connected through an edge and $i, j \in V$, k is the number of total non-zero elements in the upper triangle of $\overline{A}$, d_i and d_j are the respective degrees of nodes i and j. The assortativity is calculated using the MATLAB function defined in [67].

In some networks, nodes that have some similarity tend to have more connections [69]. There are different indices to measure the similarity, but most nodes connect to nodes that have a similar degree [70]. Therefore, the assortativity is a measurement of how nodes in a network are associating with each other. If there is similarity in the brain functional activity of ASD subjects, the association of ROIs with each other should also be similar and so is the assortativity for ASD subjects. However, due to the difference in the functional activity, the assortativity of TC subjects should be different from ASD subjects.

b: CLUSTERING COEFFICIENT
The clustering coefficient of a node is the fraction of triangles around it [71], and it measures the local connectivity of a network. For the calculation of the clustering coefficient, the adjacency matrix A is transformed to $\overline{A}$, similar to the assortativity. Then the number of triangles of each node (denoted by β_G) is calculated as follows

$$\beta_G = \mathbf{diag}(\overline{A} \times U(\overline{A}) \times \overline{A}) \tag{8}$$

where *diag* is the MATLAB function which returns the diagonal elements of the matrix and $U(\overline{A})$ is the upper triangular matrix of $\overline{A}$. Finally the clustering coefficient, C is calculated as follows

$$C = \frac{1}{f}(\sum_{i\in V} 2 \times (\frac{\beta_G(i)}{d_i \times (d_i - 1)})) \tag{9}$$

where for a network $G = (V, E)$, f is the total number of nodes in the network and d_i is the degree of node i.

The high average clustering coefficient of a network is interpreted as densely connected local clusters [72]. The clustering coefficient is more evident in the network that shows small-world properties. As brain networks have small-world properties, the clustering coefficient could help exploit if the regions tend to cluster more or less together in ASD than TC [73], [74]. Also, as mentioned in [18] ASD subjects have lower clustering coefficient than those TC subjects.

c: THE AVERAGE DEGREE OF A NETWORK
The average degree (denoted by Q) of a network is the ratio of the number of all the edges to the number of all nodes in a network and it can be calculated from the adjacency matrix $A = (a_{i,j})_{n\times n}$ as follows

$$Q = \frac{2}{f} \times \sum_{i=1}^{f} \sum_{j=1}^{f} a_{i,j} \tag{10}$$

where f is the total number of nodes in the network.

The adjacency matrix is a representation of the correlation and anti-correlation between different regions of a brain. For a particular subject type (say ASD or TC), there should be similarity in the functional activity of brain regions and the average degree of a network is expected to capture it.

We have normalized the topological centralities before applying the feature selection algorithm. We have separately normalized the centralities as follows

$$z' = \frac{z - \min(z)}{\max(z) - \min(z)} \tag{11}$$

where z is an original value and z is the normalized value.

3) FEATURE SELECTION
The efficiency of a machine learning algorithm greatly depends on features. The more discriminant the features are, the better machine learning algorithms can perform. Unnecessary features can make models complicated and overfitted while reducing the efficiency of machine learning algorithms. These problems can be addressed by using a feature selection algorithm [75]. The primary purpose of feature selection algorithms is to find the minimal subset of the most discriminate features [76] while improving the prediction accuracy of models [77].

The sequential feature selection is a very popular and straightforward feature selection algorithm. There are two variants of feature selection algorithms. One is the forward selection, where features are sequentially added to a subset of features selected from the original feature set until adding any further features doesn't increase the classification accuracy. The second one is the backward feature selection, where the unnecessary features are removed sequentially from the original feature set until removing any further features doesn't increase the classification accuracy. We have used the backward sequential feature selection algorithm in this study. Specifically, MATLAB function ''sequentialfs'' is used to perform the backward sequential feature selection algorithm with LDA and the 10 fold cross-validation.

The ''sequentialfs'' algorithm divides the data only once during the cross-validation step and tries to optimize the classification accuracy with those sets. This algorithm often stops before reaching the optimal feature subset. To resolve this problem, we have implemented an iterative method. During each iteration, the ''sequentialfs'' is used to create a feature subset by removing redundant features from the previously remained feature subset. Then, the 10-fold cross-validation with LDA is performed on the remained feature subset.
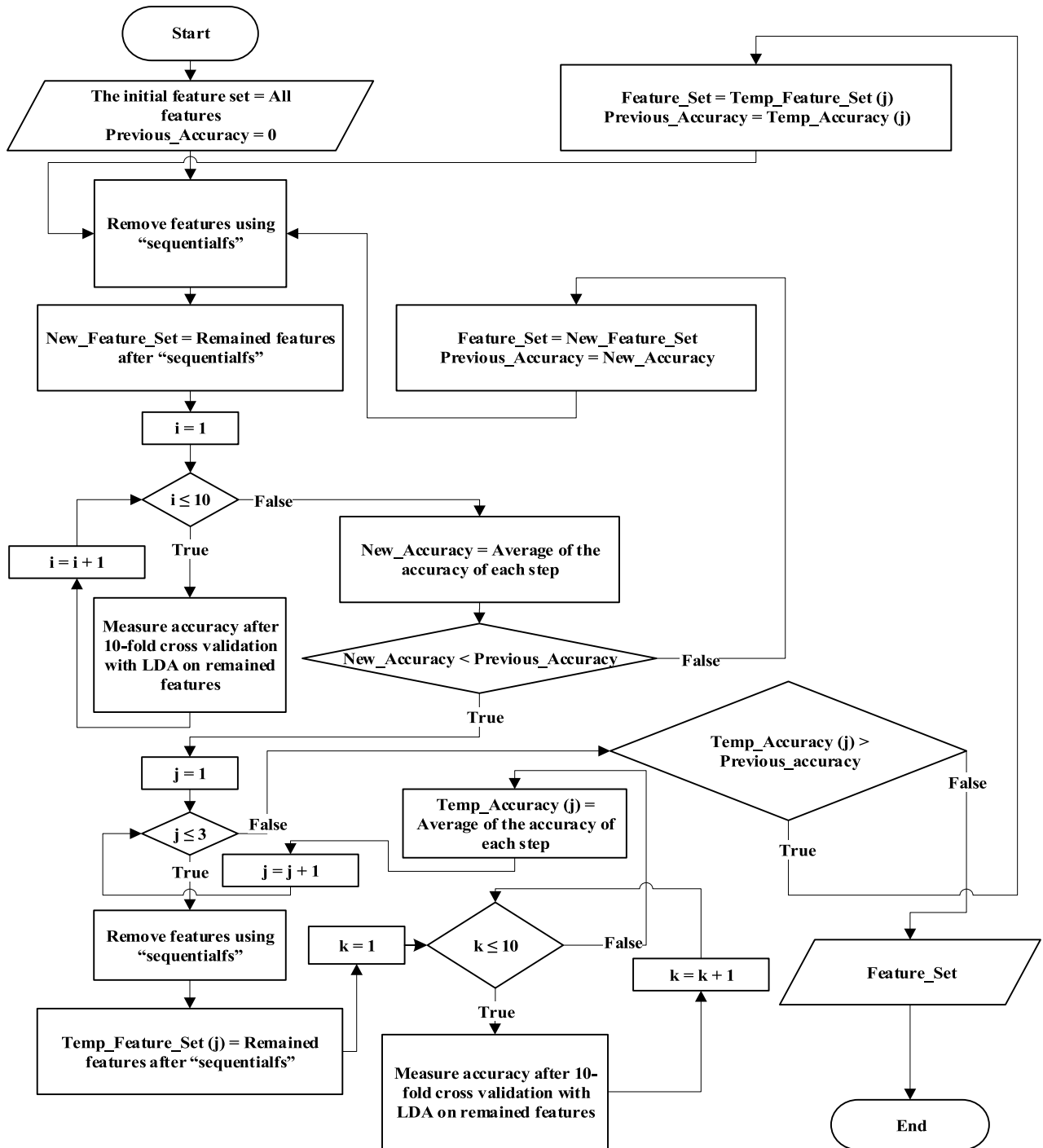
FIGURE 2. Flowchart of the feature selection algorithm. Input of the algorithm is the feature vector containing all the features and output is the minimum set of features with the maximum accuracy.

We have repeated the 10-fold cross-validation 10 times using the same feature subset, and the average of the classification accuracy of each step is considered as the classification accuracy of that subset. Running the cross-validation multiple times can ensure that the classifier isn't biased by any particular set of data. If the new accuracy, which is the accuracy of the current step after the cross-validation, is lower

than the accuracy of the previous step then, we have further removed the features using "sequentialfs" from the newly remained feature subset. We have performed the removal of feature three times, and each time "sequentialfs" is used on the previously remained feature subset. We have used this step to inspect the accuracy of the next three iterations. Because, sometimes the accuracy of the next step is lower
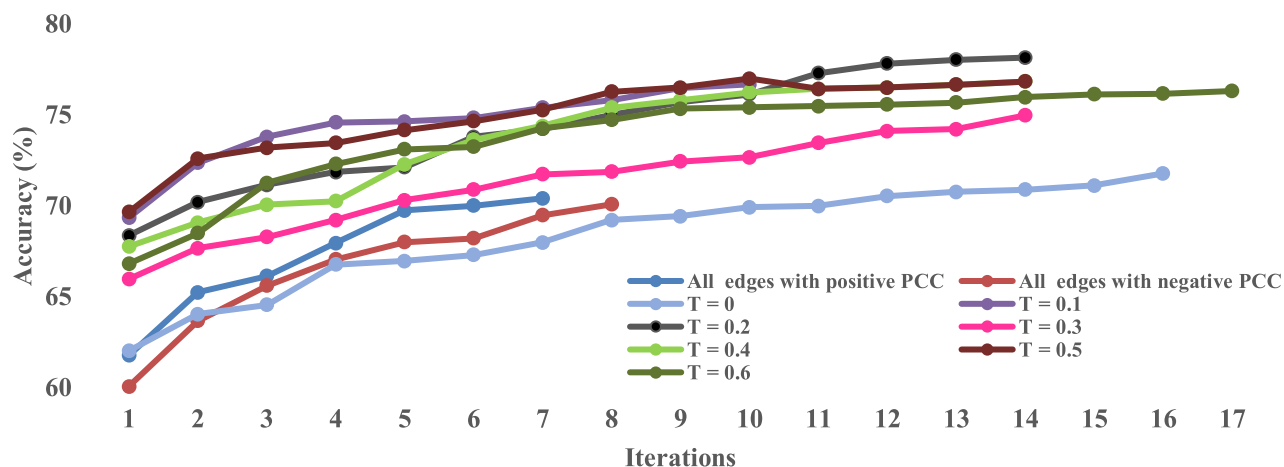
FIGURE 3. Change of the classification accuracy during each iteration of the feature selection algorithm.

than the current step, but the accuracy of the consecutive steps is better than the current step. This can ensure the algorithm wouldn't stop before reaching a minimum subset of features with the maximum accuracy. Again, the accuracy of the three steps is measured by averaging the accuracy of 10-fold cross-validation over 10 times. Now, if the accuracy of any of the three steps is higher than the new accuracy, then the features of that step are considered as the feature subset for the next iteration. However, if the new accuracy is lower than the previous accuracy and the accuracy of the following three iterations are also lower than the new accuracy, the current feature subset is considered to be the final set of features for classifiers. The feature selection algorithm is illustrated in Fig. 2.

One of the main reasons that machine learning algorithms are overfitted is by using high dimensional feature sets [22]. Most times, the study of the neuroimages includes a high dimensional feature set due to the use of a large number of voxels, and ROIs. As a result, there are noise or unnecessary features in the feature set. The noise in the feature set profoundly biases the performance of machine learning algorithms. Machine learning algorithms try to find a pattern in the feature set. However, if there are too many noises in the feature set then machine learning algorithms search for a pattern in the noise [78], which isn't an actual representation of data. Therefore, excessive features overfit machine learning algorithms by introducing noise into the feature set.

It can be summarized from Table 3 that the number of selected features has reduced significantly from the initial 267 raw features after applying the feature selection algorithm. Fig. 3 shows the change of the classification accuracy during each iteration of the feature selection algorithm. From Fig. 3, we can see that the classification accuracy has increased by removing the noises from the feature set. Fig. 4 shows a comparison of the classification accuracy with the error bars before and after applying the feature selection algorithm for different thresholding conditions. From Fig. 4 we can say that the classification accuracy has

TABLE 3. Number of features selected after using feature selection algorithm.

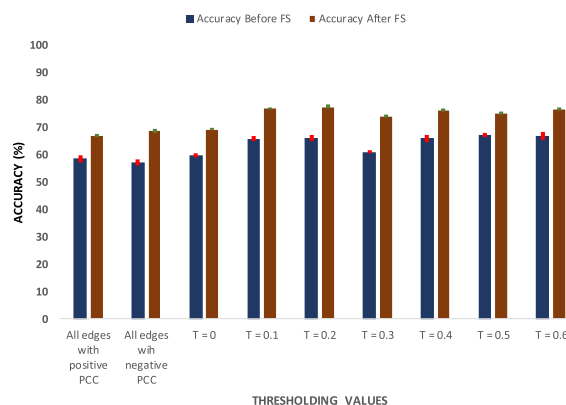| Thresholding Condition	Number Of Selected Features After Feature Selection
All edges with positive PCC	88
All edges with negative PCC	76
$T = 0$	66
$T = 0.1$	103
$T = 0.2$	62
$T = 0.3$	78
$T = 0.4$	77
$T = 0.5$	111
$T = 0.6$	37

FIGURE 4. The classification accuracy of LDA before and after applying the feature selection (FS) algorithm.

increased for all the thresholding conditions after applying the feature selection algorithm, which indicates that our proposed method can avoid the overfitting problem.

III. RESULTS AND DISCUSSION
Starting with the full spectra and topology centralities from brain networks of 871 subjects in ABIDE 1, we have applied the feature selection method to select features and then train

TABLE 4. Comparison of different thresholding values.

Thresholding Condition	LDA (%)		LR (%)		SVM (%)		KNN (%)		NN (%)	
	ACC (stdv)	AUC (stdv)	ACC (stdv)	AUC (stdv)	ACC (stdv)	AUC (stdv)	ACC (stdv)	AUC (stdv)	ACC (stdv)	AUC (stdv)
All edges with positive PCC	67.1 (0.7)	73.7 (0.5)	68.1 (0.6)	73.7 (0.8)	66.4 (0.3)	71.1 (0.3)	65.1 (0.6)	73.6 (0.8)	66.0 (4.5)	72.0 (4.2)
All edges with negative PCC	68.8 (0.7)	73.5 (0.5)	68.1 (0.8)	73.4 (0.5)	65.9 (0.5)	70.3 (0.7)	63.2 (0.8)	71.2 (0.4)	64.4 (5.9)	68.7 (7.8)
$T = 0$	69.5 (0.4)	75.5 (0.5)	70.0 (0.8)	75.7 (0.8)	65.5 (0.5)	70.2 (0.4)	62.0 (0.9)	70.5 (0.5)	66.0 (4.5)	73.0 (2.8)
$T = 0.1$	77.0 (0.4)	81.8 (0.6)	75.9 (0.5)	81.1 (0.6)	75.4 (0.8)	80.8 (0.4)	72.4 (0.3)	79.8 (0.4)	71.3 (5.8)	77.5 (5.6)
$T = 0.2$	**77.7 (0.6)**	**83.1 (0.3)**	**76.6 (0.6)**	**82.9 (0.3)**	75.5 (0.4)	80.6 (0.5)	**73.7 (0.8)**	**81.3 (0.5)**	**71.7 (2.9)**	**78.7 (3.3)**
$T = 0.3$	74.1 (0.5)	77.9 (0.3)	73.8 (0.7)	77.8 (0.4)	71.3 (0.3)	78.2 (0.4)	71.5 (0.8)	78.1 (0.6)	68.3 (4.0)	74.5 (3.3)
$T = 0.4$	76.4 (0.7)	81.1 (0.6)	75.8 (0.7)	80.8 (0.4)	**75.7 (0.4)**	**80.9 (0.3)**	72.2 (0.7)	79.7 (0.5)	71.3 (4.8)	77.1 (4.5)
$T = 0.5$	75.3 (0.7)	80.4 (0.5)	74.5 (0.7)	79.7 (0.5)	75.2 (0.5)	79.9 (0.3)	72.2 (0.5)	79.2 (0.4)	70.1 (3.1)	76.9 (4.0)
$T = 0.6$	76.8 (0.5)	81.4 (0.5)	76.6 (0.2)	80.9 (0.7)	75.6 (0.4)	80.8 (0.5)	73.0 (0.6)	80.5 (0.5)	68.4 (4.8)	75.5 (3.9)

different machine learning algorithms with the selected features. In this section, we discuss the experimental results of our study.

The features we have used in this study are derived from the connectivity matrix after removing weak edges. Actually, it is crucial to find an optimal thresholding value which removes most weak edges while losing least strong edges.In our study, to find the optimal thresholding value we have experimented with different thresholding values **T** from **0** to **0.6**, with the increment of **0.1**. To emphasize the necessity of combining both the negative PCC values and positive PCC values, we have also experimented with edges with only positive PCC values and the edges with only negative PCC values. To calculate the adjacency matrix, $A = (a_{i,j})$ for edges with only negative PCC values, formula (2) is modified as follows

$$a_{i,j} = \begin{cases} 0, & if \ cm_{i,j} > 0 \\ 1, & if \ cm_{i,j} < 0 \end{cases} \qquad (12)$$

Note that all adjacency matrices derived with only positive or only negative PCC values have an eigenvalue of zero, which is discarded before applying the feature selection.

Our hypothesis is that the features selected with our proposed method can improve the performance of all machined learning method. Therefore, we have applied our selected features to several commonly used machine learning methods, which include LDA, logistic regression (LR), support vector machine (SVM), K-nearest neighbor (KNN) and neural network (NN), to classify ASD and TC subjects. LDA, LR, SVM, and KNN are implemented in MATLAB while NN is implemented in PyCharm with the python.

KNN is implemented with the cosine as the distance metric while SVM is implemented with the medium Gaussian kernel. LR with the default value is implemented on the classification learner app of MATLAB [79]. NN with one

TABLE 5. Accuracy comparison of proposed method and state of the art classification methods.

Methods	Accuracy (%)
Wong et al. [8]	71.1
Dvornek et al. [6]	70.1
Heinsfeld et al. [23]	70.0
Eslami et al. [24]	70.1
Abraham et al. [27]	66.8
Khosla et al. [28]	73.3
Parisot et al. [29]	69.5
Xing et al. [69]	66.8
Proposed study with NN	71.7
Proposed study with KNN	73.7
Proposed study with SVM	75.7
Proposed study with LR	77.0
Proposed study with LDA	77.7

input layer, one hidden layer, and one output layer is built with TensorFlow. In the input layer, the number of neurons equals the number of selected features. "Softmax" is used as the activation function after the input layer. Then a fully connected hidden layer with 2 neurons is used. Rather than using the stochastic gradient descent, we have used the adam optimizer to update the weights. For machine learning algorithms, we have used the 10-fold cross-validation to measure accuracy (ACC) and the area under the receiver operating characteristic (ROC) curve (AUC). For NN we have split the data into a training set (80%), a testing set (10%), and a validation set (10%). We have used the training set and testing set to create the NN model and the validation set to measure the final accuracy. To show the stability of the classification process, we have repeated experiments 10 times for all machine learning algorithms. The average ACC and AUC, along with the standard deviation (stdv) of experiments are shown in Table 4.

TABLE 6. Classification accuracy and AUC of the different sites of ABIDE 1.

Sites	Total Subjects		Total Subjects	Features After FS	LDA (%)		LR (%)	
	ASD	TC			ACC	AUC	ACC	AUC
PITT	24	26	50	15	100	100	100	100
OLIN	14	14	28	14	100	100	92.9	99.0
OHSU	12	13	25	2	100	100	100	100
SDSU	8	19	27	7	92.6	96.0	96.3	99.0
TRINITY	19	25	44	19	97.7	100	97.7	100
UM 1	34	52	87	79	97.7	97.0	87.2	90.0
UM 2	13	21	34	14	100	100	97.1	99.0
UM	47	73	120	54	92.5	98.0	94.2	95.0
USM	43	24	67	24	98.5	100	97.0	99.0
YALE	22	19	41	5	100	100	100	100
CMU	6	5	11	3	100	100	100	100
LEUVEN 1	14	14	28	11	96.4	100	96.4	100
LEUVEN 2	12	16	28	13	100	100	100	100
LEUVEN	26	30	56	27	100	100	96.4	100
KKI	12	21	33	7	97.0	100	93.9	99.0
NYU	74	98	172	5	99.4	100	100	100
STANFORD	12	13	25	12	100	100	100	100
UCLA 1	37	27	64	13	100	100	96.9	100
UCLA 2	11	10	21	9	100	100	100	100
UCLA	48	37	85	17	100	100	100	100
MAX_MUN	19	27	46	24	100	100	100	100
CALTECH	5	10	15	6	93.3	100	93.3	100
SBL	12	14	26	1	100	100	100	100

Machine learning algorithms perform better when the features are discriminating. The more discriminant the features are, the better machine learning algorithms perform. The discriminate property of the proposed features can be examined in Table 4. From Table 4, we can see that removing the weak edges produce better results than either all the edges with positive PCC values or all the edges with negative PCC values. All machine learning algorithms achieved their best performance with the thresholding value of 0.2. LDA with the thresholding value of 0.2 outperformed the state-of-the-art diagnosis processes. Even ACCs of LR, KNN, SVM, and NN are better than the state-of-the-art methods. These results indicate that even using the most straightforward machine learning algorithms, we have achieved a better diagnosis process than the state-of-the-art methods.

Table 5 shows the comparison of the classification accuracy of our proposed method and state-of-the-art methods. One of the major problems of ASD studies is the inconsistency of subjects used in the research projects, which makes the comparison very hard. To be consistent, we have compared our work with the studies that have used the entire ABIDE 1 dataset. From Table 5, we can summarize that with our proposed features all machine learning methods can achieve a better classification accuracy than the state-of-the-art methods.

The inter-site variation of ABIDE 1 dataset is very prominent, as it covers a wide range of age groups, sexes, scanning parameters, and scanners (Table 1 and Table 2). This represents the real-world scenario, where the scanner or scanning parameters cannot be controlled uniformly at different sites or institutions. However, for a particular institution, they are very unlikely to have a prominent difference in the scanner or the scanning parameters. Therefore, the classification of the intra-site classes is also important. We have also conducted the experiments on the 17 sites of ABIDE 1 database separately. For the intra-site experiments, we have kept the threshold value $T = 0.2$ to be consistent. We have applied the feature selection method to the dataset from each site, separately. In all the cases, the number of selected features is smaller than the number of subjects in the datasets, which again illustrates the efficiency of the feature selection algorithm to avoid the overfitting issue. ACC and AUC are calculated based on the 10-fold cross-validation with LDA and LR and are shown in Table 6. UCLA, UM, and LEUVEN sites have two different datasets. We have calculated the accuracy based on each dataset separately and, as well as the entire dataset. From Table 5, it can be seen that our defined and selected features are greatly beneficial to classify ASD and TC subjects in case of the intra-site datasets. Specifically, our proposed process can diagnose ASD with an average ACC of 98.5% ± 2.5% and an average AUC of 99.6% ± 1.1% for

all the sites using LDA. At some sites, the accuracy and/or the AUC have reached 100%. The efficiency of defined and selected features is illustrated by not only LDA but also LR, which also has the average ACC of 97.3% ± 3.3% and the average AUC of 99.1% ± 2.3%. Using both LDA and LR, the average ACC is much better than the average ACC of 63.0% reported in [23], and 52.0% reported in [24].

IV. CONCLUSION

In this study, we have proposed a set of new features for machine learning algorithms to diagnose ASD based on rs-fMRI images. We have constructed brain networks from rs-fMRI images with 264 ROIs as nodes and the PCC values of their pairwise time-series signals as the weight of edges. In the next step, we have defined features from the connectivity matrix. Apart from the traditional network-based features, such as topology centralities, we have proposed eigenvalues of the Laplacian matrix of brain networks as new features. Combining all these features, we have achieved higher accuracy than the state-of-the-art methods after applying a feature selection algorithm, which has also helped to improve the performance of machine learning algorithms.

To illustrate the effectiveness of the selected features we have tested with several machine learning algorithms. The classification accuracy is 77.7% for LDA. The acquired accuracy is based on ABIDE 1 dataset, which covers a wide range of different parameters, which reflects the real-world scenario. The high accuracy of intra-site data has illustrated the effectiveness and robustness of our proposed features. In summary, our proposed study can help diagnose ASD more accurately and help lessen ASD patient's burden for the long run. In the feature, more advanced machine learning techniques such as reinforcement and deep learning [80], [81] should be used with our proposed features to build better classification models.

REFERENCES

[1] *Autism Spectrum Disorder Among Children and Youth in Canada 2018*. Accessed: May 13, 2019. [Online]. Available: https://www.canada.ca/en/public-health/services/publications/diseases-conditions/autism-spectrum-disorder-children-youth-canada-2018.html

[2] C. Lord, M. Rutter, S. Goode, J. Heemsbergen, H. Jordan, L. Mawhood, and E. Schopler, "Austism diagnostic observation schedule: A standardized observation of communicative and social behavior," *J. Autism Developmental Disorders*, vol. 19, no. 2, pp. 185–212, Jun. 1989.

[3] C. Lord, M. Rutter, and A. Le Couteur, "Autism diagnostic interview-revised: A revised version of a diagnostic interview for caregivers of individuals with possible pervasive developmental disorders," *J. Autism Develop. Disorders*, vol. 24, no. 5, pp. 659–685, Oct. 1994.

[4] M. Ismail, G. Barnes, M. Nitzken, A. Switala, A. Shalaby, E. Hosseini-Asl, M. Casanova, R. Keynton, A. Khalil, and A. El-Baz, "A new deep-learning approach for early detection of shape variations in autism using structural MRI," in *Proc. IEEE Int. Conf. Image Process. (ICIP)*, Sep. 2017, pp. 1057–1061.

[5] K. Al-Jabery, T. Obafemi-Ajayi, G. R. Olbricht, T. N. Takahashi, S. Kanne, and D. Wunsch, "Ensemble statistical and subspace clustering model for analysis of autism spectrum disorder phenotypes," in *Proc. 38th Annu. Int. Conf., IEEE Eng. Med. Biol. Soc. (EMBC)*, Aug. 2016, pp. 3329–3333.

[6] N. C. Dvornek, P. Ventola, and J. S. Duncan, "Combining phenotypic and resting-state fMRI data for autism classification with recurrent neural networks," in *Proc. IEEE 15th Int. Symp. Biomed. Imag. (ISBI)*, Apr. 2018, pp. 725–728.

[7] O. Altay and M. Ulas, "Prediction of the autism spectrum disorder diagnosis with linear discriminant analysis classifier and K-nearest neighbor in children," in *Proc. 6th Int. Symp. Digit. Forensic Secur. (ISDFS)*, May 2018, pp. 1–4.

[8] E. Wong, J. S. Anderson, B. A. Zielinski, and P. T. Fletcher, "Riemannian regression and classification models of brain networks applied to autism," in *Connectomics in NeuroImaging*. Cham, Switzerland: Springer, 2018, pp. 78–87.

[9] F. Pereira, T. Mitchell, and M. Botvinick, "Machine learning classifiers and fMRI: A tutorial overview," *NeuroImage*, vol. 45, no. 1, pp. S199–S209, Mar. 2009.

[10] M. Greicius, "Resting-state functional connectivity in neuropsychiatric disorders," *Current Opinion Neurol.*, vol. 21, no. 4, pp. 424–430, Aug. 2008.

[11] D. C. Van Essen and K. Ugurbil, "The future of the human connectome," *NeuroImage*, vol. 62, no. 2, pp. 1299–1310, Aug. 2012.

[12] V. Menon, "Large-scale brain networks and psychopathology: A unifying triple network model," *Trends Cognit. Sci.*, vol. 15, no. 10, pp. 483–506, 2011.

[13] E. Bullmore and O. Sporns, "Complex brain networks: Graph theoretical analysis of structural and functional systems," *Nat. Rev. Neurosci.*, vol. 10, no. 4, pp. 186–198, Mar. 2009.

[14] M. Rubinov and O. Sporns, "Complex network measures of brain connectivity: Uses and interpretations," *NeuroImage*, vol. 52, no. 3, pp. 1059–1069, 2010.

[15] T. Iidaka, "Resting state functional magnetic resonance imaging and neural network classified autism and control," *Cortex*, vol. 63, pp. 55–67, Feb. 2015.

[16] E. Delbruck, M. Yang, A. Yassine, and E. D. Grossman, "Functional connectivity in ASD: Atypical pathways in brain networks supporting action observation and joint attention," *Brain Res.*, vol. 1706, pp. 157–165, Mar. 2019.

[17] J. A. Nielsen, B. A. Zielinski, P. T. Fletcher, N. Lange, E. D. Bigler, J. E. Lainhart, J. S. Anderson, and A. L. Alexander, "Multisite functional connectivity MRI classification of autism: ABIDE results," *Frontiers Hum. Neurosci.*, vol. 7, p. 599, Sep. 2013.

[18] J. D. Rudie, J. A. Brown, D. Beck-Pancer, L. M. Hernandez, E. L. Dennis, P. M. Thompson, S. Y. Bookheimer, and M. Dapretto, "Altered functional and structural brain network organization in autism," *NeuroImage, Clin.*, vol. 2, pp. 79–94, Jan. 2013.

[19] S. Sartipi, M. G. Shayesteh, and H. Kalbkhani, "Diagnosing of autism spectrum disorder based on GARCH variance series for rs-fMRI data," in *Proc. 9th Int. Symp. Telecommun. (IST)*, Dec. 2018, pp. 86–89.

[20] J. Wang, Q. Wang, H. Zhang, J. Chen, S. Wang, and D. Shen, "Sparse multiview task-centralized ensemble learning for ASD diagnosis based on age- and sex-related functional connectivity patterns," *IEEE Trans. Cybern.*, vol. 49, no. 8, pp. 3141–3154, Aug. 2019.

[21] T. Watanabe and G. Rees, "Brain network dynamics in high-functioning individuals with autism," *Nature Commun.*, vol. 8, no. 1, Dec. 2017, Art. no. 16048.

[22] N. Yahata, J. Morimoto, R. Hashimoto, G. Lisi, K. Shibata, Y. Kawakubo, H. Kuwabara, M. Kuroda, T. Yamada, F. Megumi, H. Imamizu, J. E. Náñez, Sr., H. Takahashi, Y. Okamoto, K. Kasai, N. Kato, Y. Sasaki, T. Watanabe, and M. Kawato, "A small number of abnormal brain connections predicts adult autism spectrum disorder," *Nature Commun.*, vol. 7, no. 1, Sep. 2016, Art. no. 11254.

[23] A. S. Heinsfeld, A. R. Franco, R. C. Craddock, A. Buchweitz, and F. Meneguzzi, "Identification of autism spectrum disorder using deep learning and the ABIDE dataset," *NeuroImage, Clin.*, vol. 17, pp. 16–23, Jan. 2018.

[24] T. Eslami, V. Mirjalili, A. Fong, A. Laird, and F. Saeed, "ASD-DiagNet: A hybrid learning approach for detection of Autism Spectrum Disorder using fMRI data," 2019, *arXiv:1904.07577v1*. [Online]. Available: https://arxiv.org/abs/1904.07577

[25] M. R. Arbabshirani, S. Plis, J. Sui, and V. D. Calhoun, "Single subject prediction of brain disorders in neuroimaging: Promises and pitfalls," *NeuroImage*, vol. 145, pp. 137–165, Jan. 2017.

[26] J. D. Power, A. L. Cohen, S. M. Nelson, G. S. Wig, K. A. Barnes, J. A. Church, A. C. Vogel, T. O. Laumann, F. M. Miezin, B. L. Schlaggar, and S. E. Petersen, "Functional network organization of the human brain," *Neuron*, vol. 72, no. 4, pp. 665–678, Nov. 2011.

[27] A. Abraham, M. P. Milham, A. Di Martino, R. C. Craddock, D. Samaras, B. Thirion, and G. Varoquaux, "Deriving reproducible biomarkers from multi-site resting-state data: An autism-based example," *NeuroImage*, vol. 147, pp. 736–745, Feb. 2017.

[28] M. Khosla, K. Jamison, A. Kuceyeski, and M. R. Sabuncu, "3D convolutional neural networks for classification of functional connectomes," in *Deep Learning in Medical Image Analysis and Multimodal Learning for Clinical Decision Support*. Cham, Switzerland: Springer, 2018, pp. 137–145.

[29] S. Parisot, S. I. Ktena, E. Ferrante, M. Lee, R. G. Moreno, B. Glocker, and D. Rueckert, "Spectral graph convolutions for population-based disease prediction," in *Medical Image Computing and Computer Assisted Intervention*, Cham, Switzerland: Springer, 2017, pp. 177–185.

[30] X. Xing, J. Ji, and Y. Yao, "Convolutional neural network with element-wise filters to extract hierarchical topological features for brain networks," in *Proc. IEEE Int. Conf. Bioinforma. Biomed. (BIBM)*, Dec. 2018, pp. 780–783.

[31] A. Di Martino *et al.*, "The autism brain imaging data exchange: Towards a large-scale evaluation of the intrinsic brain architecture in autism," *Mol. Psychiatry*, vol. 19, no. 6, pp. 659–667, 2014.

[32] R. W. Cox, "AFNI: Software for analysis and visualization of functional magnetic resonance neuroimages," *Comput. Biomed. Res.*, vol. 29, no. 3, pp. 162–173, Jun. 1996.

[33] M. Jenkinson, C. F. Beckmann, T. E. Behrens, M. W. Woolrich, and S. M. Smith, "FSL," *NeuroImage*, vol. 62, no. 2, pp. 782–790, 2012.

[34] M. Jenkinson, P. Bannister, M. Brady, and S. Smith, "Improved optimization for the robust and accurate linear registration and motion correction of brain images," *NeuroImage*, vol. 17, no. 2, pp. 825–841, Oct. 2002.

[35] M. Jenkinson and S. Smith, "A global optimisation method for robust affine registration of brain images," *Med. Image Anal.*, vol. 5, no. 2, pp. 143–156, Jun. 2001.

[36] Y. Zhang, M. Brady, and S. Smith, "Segmentation of brain MR images through a hidden Markov random field model and the expectation-maximization algorithm," *IEEE Trans. Med. Imag.*, vol. 20, no. 1, pp. 45–57, Jan. 2001.

[37] J. Wang, L. Wang, Y. Zang, H. Yang, H. Tang, Q. Gong, Z. Chen, C. Zhu, and Y. He, "Parcellation-dependent small-world brain functional networks: A resting-state fMRI study," *Hum. Brain Mapp.*, vol. 30, no. 5, pp. 1511–1523, May 2009.

[38] A. Zalesky, A. Fornito, L. Cocchi, M. Yücel, C. Pantelis, E. T. Bullmore, and I. H. Harding, "Whole-brain anatomical networks: Does the choice of nodes matter?" *NeuroImage*, vol. 50, no. 3, pp. 970–983, 2010.

[39] C. T. Butts, "Revisiting the foundations of network analysis," *Science*, vol. 325, no. 5939, pp. 414–416, Jul. 2009.

[40] A. Hahamy, M. Behrmann, and R. Malach, "The idiosyncratic brain: Distortion of spontaneous connectivity patterns in autism spectrum disorder," *Nature Neurosci.*, vol. 18, no. 2, pp. 302–309, Jan. 2015.

[41] J. J. Paakki, J. Rahko, X. Long, I. Moilanen, O. Tervonen, J. Nikkinen, T. Starck, J. Remes, T. Hurtig, H. Haapsamo, K. Jussila, S. Kuusikko-Gauffin, M.-L. Mattila, Y. Zang, and V. Kiviniemi, "Alterations in regional homogeneity of resting-state brain activity in autism spectrum disorders," *Brain Res.*, vol. 1321, pp. 169–179, Mar. 2010.

[42] Z. Long, X. Duan, D. Mantini, and H. Chen, "Alteration of functional connectivity in autism spectrum disorder: Effect of age and anatomical distance," *Sci. Rep.*, vol. 6, no. 1, May 2016, Art. no. 26527.

[43] S. Mueller, D. Wang, M. D. Fox, B. T. T. Yeo, J. Sepulcre, M. R. Sabuncu, R. Shafee, J. Lu, and H. Liu, "Individual variability in functional connectivity architecture of the human brain," *Neuron*, vol. 77, no. 3, pp. 586–595, 2013.

[44] P. Fransson, U. Åden, M. Blennow, and H. Lagercrantz, "The functional architecture of the infant brain as revealed by resting-state fMRI," *Cerebral Cortex*, vol. 21, no. 1, pp. 145–154, Jan. 2011.

[45] M. W. Cole, S. Pathak, and W. Schneider, "Identifying the brain's most globally connected regions," *NeuroImage*, vol. 49, no. 4, pp. 3132–3148, Feb. 2010.

[46] P. Hagmann, L. Cammoun, X. Gigandet, R. Meuli, C. J. Honey, Van J. Wedeen, and O. Sporns, "Mapping the structural core of human cerebral cortex," *PLoS Biol.*, vol. 6, no. 7, p. e159, Jul. 2008.

[47] F. Megumi, A. Yamashita, M. Kawato, and H. Imamizu, "Functional MRI neurofeedback training on connectivity between two regions induces long-lasting changes in intrinsic functional network," *Front. Hum. Neurosci.*, vol. 9, p. 160, Mar. 2015.

[48] R. S. Desikan, F. Ségonne, B. Fischl, B. T. Quinn, B. C. Dickerson, D. Blacker, R. L. Buckner, A. M. Dale, R. P. Maguire, B. T. Hyman, M. S. Albert, and R. J. Killiany, "An automated labeling system for subdividing the human cerebral cortex on MRI scans into gyral based regions of interest," *NeuroImage*, vol. 31, no. 3, pp. 968–980, Jul. 2006.

[49] N. Tzourio-Mazoyer, B. Landeau, D. Papathanassiou, F. Crivello, O. Etard, N. Delcroix, B. Mazoyer, and M. Joliot, "Automated anatomical labeling of activations in SPM using a macroscopic anatomical parcellation of the MNI MRI single-subject brain," *NeuroImage*, vol. 15, no. 1, pp. 273–289, 2002.

[50] A. Klein and J. Tourville, "101 labeled brain images and a consistent human cortical labeling protocol," *Frontiers Neurosci.*, vol. 6, p. 171, Dec. 2012.

[51] C. Destrieux, B. Fischl, A. Dale, and E. Halgren, "Automatic parcellation of human cortical gyri and sulci using standard anatomical nomenclature," *NeuroImage*, vol. 53, no. 1, pp. 1–15, Oct. 2010.

[52] D. C. Rojas, E. Peterson, E. Winterrowd, M. L. Reite, S. J. Rogers, and J. R. Tregellas, "Regional gray matter volumetric changes in autism associated with social and repetitive behavior symptoms," *BMC Psychiatry*, vol. 6, no. 1, Dec. 2006, Art. no. 56.

[53] E. L. Dennis, N. Jahanshad, J. D. Rudie, J. A. Brown, K. Johnson, K. L. McMahon, G. I. de Zubicaray, G. Montgomery, N. G. Martin, M. J. Wright, S. Y. Bookheimer, M. Dapretto, A. W. Toga, and P. M. Thompson, "Altered structural brain connectivity in healthy carriers of the autism risk gene, CNTNAP2," *Brain Connectivity*, vol. 1, no. 6, pp. 447–459, 2011.

[54] J. D. Lewis, A. C. Evans, J. R. Pruett, Jr., K. N. Botteron, R. C. McKinstry, L. Zwaigenbaum, A. M. Estes, D. L. Collins, P. Kostopoulos, G. Gerig, S. R. Dager, S. Paterson, R. T. Schultz, M. A. Styner, H. C. Hazlett, and J. Piven, "The emergence of network inefficiencies in infants with autism spectrum disorder," *Biol. Psychiatry*, vol. 82, no. 3, pp. 176–185, Aug. 2017.

[55] C. J. Goch, B. Stieltjes, R. Henze, J. Hering, L. Poustka, H.-P. Meinzer, and K. H. Maier-Hein, "Quantification of changes in language-related brain areas in autism spectrum disorders using large-scale network analysis," *Int. J. Comput. Assist. Radiol. Surg.*, vol. 9, no. 3, pp. 357–365, May 2014.

[56] R. Henson, "Analysis of fMRI timeseries: Linear time-invariant models, event-related fMRI and optimal experimental design," in *Human Brain Function*, R. S. J. Frackowiak, K. J. Friston, C. D. Frith, R. J. Dolan, C. J. Price, S. Zeki, J. T. Ashburner, and W. D. Penny, Eds., 2nd ed. London, U.K.: Elsevier, 2004, pp. 793–822.

[57] D. Zhou, "Functional connectivity analysis of fMRI time-series data," Ph.D. dissertation, Dept. Statist., Univ. Pittsburgh, Pittsburgh, PA, USA, 2005.

[58] S. Hayasaka and P. J. Laurienti, "Comparison of characteristics between region-and voxel-based network analyses in resting-state fMRI data," *NeuroImage*, vol. 50, no. 2, pp. 499–508, Apr. 2010.

[59] J. Wang, X. Zuo, and Y. He, "Graph-based network analysis of resting-state functional MRI," *Frontiers Syst. Neurosci.*, vol. 4, no. 16, p. 16, 2010.

[60] A. J. Schwarz and J. McGonigle, "Negative edges and soft thresholding in complex network analysis of resting state functional connectivity data," *NeuroImage*, vol. 55, no. 3, pp. 1132–1146, Apr. 2011.

[61] J. A. Mumford, S. Horvath, M. C. Oldham, P. Langfelder, D. H. Geschwind, and R. A. Poldrack, "Detecting network modules in fMRI time series: A weighted network analysis approach," *NeuroImage*, vol. 52, no. 4, pp. 1465–1476, 2010.

[62] K. Gopinath, V. Krishnamurthy, R. Cabanban, and B. A. Crosson, "Hubs of anticorrelation in high-resolution resting-state functional connectivity network architecture," *Brain Connect.*, vol. 5, no. 5, pp. 267–275, Jun. 2015.

[63] L. Tian, T. Jiang, Y. Liu, C. Yu, K. Wang, Y. Zhou, M. Song, and K. Li, "The relationship within and between the extrinsic and intrinsic systems indicated by resting state correlational patterns of sensory cortices," *NeuroImage*, vol. 36, no. 3, pp. 684–690, Jul. 2007.

[64] L. Q. Uddin, A. M. C. Kelly, B. B. Biswal, F. X. Castellanos, and M. P. Milham, "Functional connectivity of default mode network components: Correlation, anticorrelation, and causality," *Hum. Brain Mapp.*, vol. 30, no. 2, pp. 625–637, Feb. 2009.

[65] F. Parente and A. Colosimo, "The role of negative links in brain networks," *Biophys. Bioeng. Lett.*, vol. 9, no. 1, pp. 1–13, Nov. 2016.

[66] X. Huang, M. Ghodsi, and H. Hassani, "A Novel similarity measure based on eigenvalue distribution," *Trans. Razmadze Math. Inst.*, vol. 170, no. 3, pp. 352–362, 2016.

[67] M. Mijalkov, E. Kakaei, J. B. Pereira, E. Westman, and G. Volpe, "BRAPH: A graph theory software for the analysis of brain connectivity," *PLoS ONE*, vol. 12, no. 8, Aug. 2017, Art. no. e0178798.

[68] M. E. J. Newman, "Assortative mixing in networks," *Phys. Rev. Lett.*, vol. 89, no. 20, p. 208701, Oct. 2002.

[69] M. Piraveenan, M. Prokopenko, and A. Zomaya, "Assortative mixing in directed biological networks," *IEEE/ACM Trans. Comput. Biol. Bioinf.*, vol. 9, no. 1, pp. 66–78, Jan./Feb. 2012.

[70] M. E. J. Newman, "Mixing patterns in networks," *Phys. Rev. E, Stat. Phys. Plasmas Fluids Relat. Interdisc. Top.*, vol. 67, no. 2, Feb. 2003, Art. no. 026126.

[71] D. J. Watts and S. H. Strogatz, "Collective dynamics of 'small-world' networks," *Nature*, vol. 393, no. 6684, pp. 440–442, 1998.

[72] K. Supekar, V. Menon, D. Rubin, M. Musen, and M. D. Greicius, "Network analysis of intrinsic functional brain connectivity in Alzheimer's disease," *PLoS Comput. Biol.*, vol. 4, no. 6, Jun. 2008, Art. no. e1000100.

[73] O. Sporns, D. R. Chialvo, M. Kaiser, and C. C. Hilgetag, "Organization, development and function of complex brain networks," *Trends Cogn. Sci.*, vol. 8, no. 9, pp. 418–425, Sep. 2004.

[74] O. Sporns, G. Tononi, and G. M. Edelman, "Theoretical neuroanatomy: Relating anatomical and functional connectivity in graphs and cortical connection matrices," *Cerebral Cortex*, vol. 10, no. 2, pp. 127–141, Feb. 2000.

[75] H. Liu, H. Motoda, R. Setiono, and Z. Zhao, "Feature selection: An ever evolving frontier in data mining," in *Proc. Feature Sel. Data Min.*, vol. 10, May 2010, pp. 4–13.

[76] J. H. Friedman, "On bias, variance, 0/1—Loss, and the curse-of-dimensionality," *Data Min. Knowl. Discovery*, vol. 1, no. 1, pp. 55–77, Mar. 1997.

[77] L. Jourdan, C. Dhaenens, and E.-G. Talbi, "A genetic algorithm for feature selection in data-mining for genetics," in *Proc. 4th Metaheuristics Int. Conf. Porto (MIC)*, Porto, Portugal, Jul. 2001, pp. 29–34.

[78] A. GÈron, *Hands-On Machine Learning with Scikit-Learn and Tensor Flow: Concepts, Tools, and Techniques to Build Intelligent Systems*, 1st ed. Newton, MA, USA: O'Reilly Media, 2017.

[79] *Train Logistic Regression Classifiers Using Classification Learner App-MATLAB & AMP; Simulink*. Accessed: Jun. 3, 2019. [Online]. Available: https://www.mathworks.com/help/stats/train-logistic-regression-classifiers-in-classification-learner-app.html.

[80] S. Otoum, B. Kantarci, and H. Mouftah, "Empowering reinforcement learning on big sensed data for intrusion detection," in *Proc. IEEE Int. Conf. Commun. (ICC)*, May 2019, pp. 1–7.

[81] S. Otoum, B. Kantarci, and H. T. Mouftah, "On the feasibility of deep learning in sensor network intrusion detection," *IEEE Netw. Lett.*, vol. 1, no. 2, pp. 68–71, Jun. 2019.

LINGKAI TANG received the M.Sc. degree in mechanical engineering from the University of Saskatchewan, Saskatoon, Canada, in 2019. He is currently pursuing the Ph.D. degree in biomedical engineering with Western University, London, Canada. His research interests include diseases related to brain images and brain network analysis.

SAKIB MOSTAFA received the B.Sc. degree in electronics and communication engineering from the Khulna University of Engineering and Technology, Bangladesh, in 2016. His undergraduate research involved simulation study of nonlinear ultrasound imaging. He was also involved in image encryption, 3D data alignment, and reconstruction. His previous studies were presented in ICIEV-ISCMHT 2017, ICIEV 2016, WIECON-ECE 2016, and WIECON-ECE 2015. He is currently involved in brain disease detection using machine learning and deep learning, where he is working to develop new methods for the diagnosis of disease and the detection of biomarkers. His research interests include image processing, artificial intelligence, deep learning, and complex network analysis.

FANG-XIANG WU received the B.Sc. and M.Sc. degrees in applied mathematics from the Dalian University of Technology, in 1993 and 1990, respectively, the first Ph.D. degree in control theory and its applications from Northwestern Polytechnical University, in 1998, and the second Ph.D. degree in bioinformatics and computational biology from the University of Saskatchewan (U of S), in August 2004. From September 2004 to August 2005, he was a Postdoctoral Fellow with the Biomedical Research Center, Laval University. He is currently a Full Professor with the Department of Computer Science, the Division of Biomedical Engineering, and the Department of Mechanical Engineering, U of S. So far, he has published more than 360 refereed journal/conference articles. His research interests mainly include artificial intelligence/machine learning, computational biology and bioinformatics, medical image analytics, and complex network analytics. He has been invited to give research talks in about 80 international conferences or academic institutes worldwide. He is serving as an Editorial Board Member for six international journals, as the Guest Editor for numerous international journals, and as the Program Committee Chair or Member for over 30 international conferences.

• • •